Journal of Materials Chemistry C

Accepted Manuscript

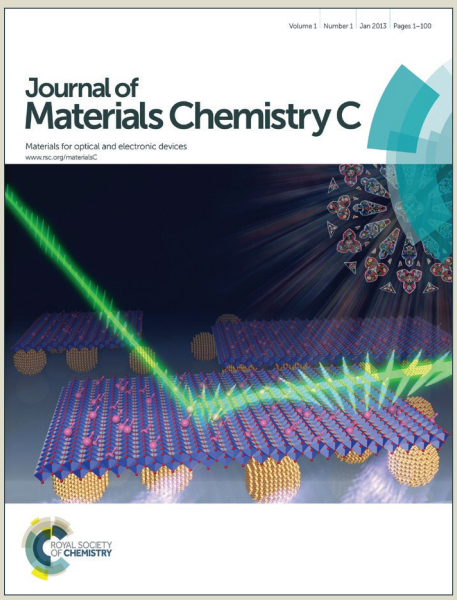

ROYAL SOCIETY OF CHEMISTRY

www.rsc.org/materialsC

Equivalent energy-level structures in stacked metamaterials

Chuanbao Liu[1], Yang Bai[1,*], Ji Zhou[2], Qian Zhao[3], Yu Yan[1], Jinxu Li[1], Yanjing Su[1] and Lijie Qiao[1]

[1]Key Laboratory of Environmental Fracture (Ministry of Education), University of Science and Technology Beijing, Beijing 100083, China

[2] State Key Laboratory of New Ceramics and Fine Processing, Tsinghua University, Beijing 100084, China

3 State Key Laboratory of Tribology, Department of Mechanical Engineering, Tsinghua University, Beijing 100084, China

Abstract. The exotic properties of metamaterials originate from the artificial metallic structure, but they indeed behave as an effective medium in the operating frequency range. Correspondingly the unit cell was called meta-atom, but its relation with real atom was not discussed substantially. In this paper, we studied a stacked fishnet meatmaterial in optical frequency range and founded a basic relationship between the meta-atom and the real atom. The characteristic frequency of meta-atoms behaves just as the energy level of real atoms, which splits with the stacked meta-atom number, converges with the atom spacing and is sensitive to the center dielectric layer features. This work will help people recognizing metamaterial physics in a view of solid-state physics and guide metamaterial design through quantum mechanical methods.

***Corresponding author.** Prof. Y. Bai Email: baiy@mater.ustb.edu.cn

Introduction

The birth of electromagnetic metamaterials at the turn of the century began a new page for materials. At first of their appearance, the left-handed property was realized with backward wave propagation [1], negative refractive index [2-4], and other exotic electromagnetic properties not existing in normal materials. Such materials filled the gap in traditional electromagnetic wave theories and provided another means of manipulating electromagnetic wave properties such as amplitude, polarization [5,6] and wavefront [7-9]. Later, many novel functions were successively developed, including subwavelength imaging [10,11], electromagnetic cloaking [12-14], and perfect absorption [15,16].

The unusual electromagnetic properties of metamaterials originate from the features of their artificial metal structures, including the shape and size, rather than being inherent in the material. However, macroscopically, metamaterials behave as an effective medium in the operating frequency range because the unit-cell size is much smaller than the characteristic wavelength. Correspondingly, the unit cell is called a meta-atom [17,18] or meta-molecule [19], but its relationship to the real atom is still an open question. Liu et al. studied the split of frequency spectrum in a multiple meta-atom system, which was similar to the split of energy level for real atom [19,20]. Nevertheless, the phenomenon of split was only discussed in fundamental mode, high-order modes and the relationship between different modes were not taken into account. García-Meca et al. ingeniously designed a fishnet metamaterial with a high figure of merit (FOM) in high-order mode, but the split of characteristic frequencies

was ignored [21]. In this paper, we systematically researched the split of characteristic frequencies, as well the formation, convergence and modulation of quasi-continuous bands in both the fundamental mode and high-order modes band gradually, so that an analogous relationship was fundamentally established between the energy level of the real atom and the characteristic frequency of the meta-atom.

Surface plasmon polaritons (SPPs) theory of fishnet structure

In this work, we studied a typical polarization-independent fishnet metamaterial consisting of alternating metal and dielectric layers, as shown in Fig. 1. For this kind of fishnet structure, across the visible spectrum, surface plasmon polaritons (SPPs) played a very important role in the transmission features, such as extraordinary optical transmission and negative refractive index [22]. The SPPs contained two parts, internal surface plasmon polaritons (I-SPPs) propagating along internal metal-dielectric interfaces induced magnetic resonance and external plasmon polaritons (E-SPPs) propagating along external metal-dielectric interfaces combined with hole's size and periodicity codetermining the electric response whose characters are similar to the single layer of Ag mesh film [23].

According to an approximate model [24,25], the relationship between the SPP k_{spp} and vacuum k_0 wave vectors can be deduced by using the method of transmission matrix based on the continuity of tangential electric and magnetic field at interfaces. For a single-layer fishnet structure, the characteristic equation was determined from the following:

$$[(\frac{k_2}{\varepsilon_2}-\frac{k_3}{\varepsilon_3})(k_1+\frac{k_2}{\varepsilon_2})e^{(k_2t-k_3d/2)}+(\frac{k_2}{\varepsilon_2}+\frac{k_3}{\varepsilon_3})(k_1-\frac{k_2}{\varepsilon_2})e^{(-k_2t-k_3d/2)}]^2 -$$
$$[(\frac{k_2}{\varepsilon_2}+\frac{k_3}{\varepsilon_3})(k_1+\frac{k_2}{\varepsilon_2})e^{(k_2t+k_3d/2)}+(\frac{k_2}{\varepsilon_2}-\frac{k_3}{\varepsilon_3})(k_1-\frac{k_2}{\varepsilon_2})e^{(-k_2t+k_3d/2)}]^2=0. \quad (1)$$

where $k_i=\sqrt{k_{spp}^2-\varepsilon_i k_0^2}$ (i=1, 2, 3) is the wave-vector component perpendicular to the interface, and the subscript numbers represent the vacuum, metal and dielectric, respectively. For a fishnet structure, the conservation of momentum and energy between the light and SPP [26] should be satisfied by the following equation:

$$\left|k_{spp}\right|=\left|G_{i,j}\right|=\left|k_0\sin\phi+i\frac{2\pi}{a_x}+j\frac{2\pi}{a_y}\right|. \quad (2)$$

where ϕ is the incident angle and both i and j are integers. Notably, the orthogonal modes cannot be excited for a polarized incidence because the magnetic resonance is polarization dependent.

Metamaterial model and simulation process

The fishnet structure consisted of alternating metal and dielectric layers, as shown in Fig. 1. To alleviate any losses, silver, with a plasma frequency of $\omega_p=1.37\times10^{16}$/s and a collision frequency of $\omega_c=8.5\times10^{13}$/s [21], was selected as the metal. The dielectric layer was set to n=2.0, consistent with ZnO [27]. The unit cell shown in the inset of Fig. 1 can be regarded as a meta-atom which had an identical configuration in the x- and y- directions. The unit cell of a single-layer fishnet structure exhibited the following geometrical parameters: $w_x=w_y=100$ nm, $a_x=a_y=240$ nm, t=50 nm, and d=32 nm. In the simulation, the wave propagates in the z-direction. The electromagnetic properties were simulated using CST Microwave Studio software. The metamaterials were characterized on the basis of transmission T, reflection R and

absorption A, as well the further retrieved effective parameters [28,29], including refractive index n_{eff}, impedance Z_{eff}, permeability μ_{eff}, and permittivity ε_{eff}.

Results and Discussions

Characteristic frequencies of a single meta-atom

Frequency spectra for single meta-atom contain a series of characteristic frequencies at which the electromagnetic wave propagates through the metamaterial in a left-handed manner instead of being forbidden (Fig. 2 (a)). The features were confirmed by the retrieved material parameters (Fig. 2 (b)-(e)) and the dynamic field distribution. The pass-band originates from the coexisting negative permittivity and permeability produced by electric resonance and magnetic resonance, respectively, with the latter playing a key role. Besides, the maximum transmission was determined by localized resonance (L-R), the corresponding frequency was very closed to the frequency of real(ε_{eff}) = 0 [22].

Fig. 2 (a) shows that the resonance frequencies for the (1,0) I-SPP, (1,1) I-SPP and (2,0) I-SPP were 401 THz, 507 THz and 650 THz, respectively, which agrees well with the numerically calculated results for 381 THz, 511 THz and 657 THz, respectively, as shown in Fig. 2(g) which are based on an approximate model. The I-SPP propagation modes were clear in magnetic field H_y distribution maps for the middle plane of the dielectric layer (Fig. 2(f)). For (1,0) and (2,0) I-SPPs, H_y presents a wavelike feature with different wavelengths along the x-direction [30,31]. For (1,1) I-SPP, the H_y waveform was along both the x- and y- directions.

Here, the characteristic frequency bands for a meta-atom can be regarded as the

energy levels of a real atom equivalently. An energy levels refers to a state in which an electron with a certain energy occupies a specific orbit, whereas the characteristic frequency band relates to an electromagnetic wave at a certain frequency propagating through the metamaterial with some specific symmetry, where the wave at a certain frequency is also regarded as a photon with a certain energy. Hence, from an energy-level viewpoint, the meta-atom behaves as a real atom.

Energy level splitting with meta-atom number

For an N-layer fishnet structure, N tightly stacked meta-atoms can be regarded as N neighbouring atoms whose strong coupling play an important role in electromagnetic characteristics (see ESI for details). For example, for two meta-atoms, each I-SPP exhibits two characteristic frequencies (Fig. 3 (a)), whose feature was confirmed with the aid of magnetic field H_y distribution maps and the numerical calculation in Fig. 2(h), and they are marked by superscripts. This phenomenon is similar to the energy level splitting when two real atoms gradually approach each other, where the overlap of their electron wavefunctions follows Pauli's exclusion principle. If more meta-atoms are stacked, the (1,0) and (1,1) I-SPP modes go on splitting (Fig. 3 (b)-(d)) and the number of submodes in each I-SPP is always equal to the meta-atom number (Fig. 3 (e)). It is because that the number of internal interfaces increases with increasing meta-atom numbers. However, for the localized resonance (L-R) whose characters were governed by the single layer Ag mesh film, the position of frequency hardly changed.

For real atoms, the number of energy levels is equal to the atomic number

multiplied by the degeneracy, where the degeneracies of the s and p orbitals are 1 and 3, respectively. In this work, the proposed meta-atom is polarization-independent, so the equivalent energy level splits with a degeneracy of 1, i.e. the number of I-SPP submodes equals to the meta-atomic number.

Energy band formation for numerous meta-atoms

When the I-SPPs split into submodes, the characteristic frequency range extends at both sides; however, this tendency gradually saturates and a quasi-continuous characteristic frequency band finally forms, as shown in Fig. 4 (a). On the basis of the energy band theory for real atoms, the principle of effective energy level splitting was summarized for meta-atoms, as illustrated in Fig. 4 (b). The $|f_{N,M}\rangle$ ($M \leqslant N$) expression represents the characteristic frequency of the M^{th} submode of a certain I-SPP with N meta-atoms. If another meta-atom is added, the original N submodes split into (N+1) submodes, and follow the inequality $|f_{(N+1),M}\rangle < |f_{N,M}\rangle < |f_{(N+1),(M+1)}\rangle$, which is analogous to energy level splitting in a real atom. The value $|f_{N,M}\rangle$ depends on the degree of symmetry or antisymmetry in the I-SPP modes. It increases if the H_y symmetry is high (right of Fig. 4 (c)), because the charges in the adjacent metal layers need more restoring forces to oscillate [20]; it decreases if the antisymmetry is high (left of Fig. 4 (c)). Although only the (1,0) and (1,1) I-SPPs are displayed here, we predict the principle is acceptable for other I-SPP modes.

Energy band converging with meta-atomic spacing

Similar to real atoms consisting of a nucleus and electrons, the dielectric layer in a stacked fishnet metamaterial can be regarded as the equivalent of a nucleus

surrounded by electrons oscillating in the adjacent metal layer; the meta-atomic spacing D is the central distance between adjacent dielectric layers, as shown in the inset in Fig. 5 (a). Here, the dielectric layer thickness was fixed to 32 nm. The thickness change of the intermediate metal layers determines the meta-atomic spacing.

Increasing the meta-atomic spacing causes the characteristic frequencies of the submodes in the same I-SPP to gradually converge, and they are too close to be distinguishable because D is large. For an example of five meta-atoms (Figs. 5 (a) & (b)), the characteristic frequencies of the (1,0) and (1,1) I-SPPs finally converge to 405 THz and 511 THz, respectively. These values differ slightly from those of the single meta-atom (401 THz and 507 THz). This difference stems from the metal thickness having the same order of magnitude as skin thickness, so fewer electrons participate during the oscillation, which lowers the I-SPP frequencies. Nevertheless, for real atoms, the convergence values always equals that of a single atom because its energy level is undisturbed by the finite carrier space.

If the meta-atom number is large and the spacing is small enough, the characteristic frequency bands of (1,0) and (1,1) I-SPPs will overlap. For example as D=62nm, the characteristic frequencies of some submodes in the (1,0) and (1,1) I-SPPs intersect and no longer correspond to their original characteristic frequency bands. Within the overlap range, such as 458 THz, the magnetic field H_y distribution differs for each layer (left of Fig. 5 (a)), and the (1,1) and (1,0) I-SPP modes appears alternately in these dielectric layers. This trait is similar to orbital overlap in real atoms, such as for

the 2s and 2p orbitals of silicon (inset of Fig. 5 (b)).

Effect of dielectric layer features

The characteristic frequency bands of stacked meta-atoms are also sensitive to the features of dielectric layer. Fig. 6 shows the characteristic frequency as a function of the relative permittivity of the dielectric layer for 27 meta-atoms, where the characteristic frequencies have become quasi-continuous bands. An increase in the dielectric layer permittivity moves the characteristic frequency bands of (1,0) and (1,1) I-SPPs towards lower frequencies.

The dielectric layer features also determine whether the metamaterial behaves as a pass or forbidden band at a certain characteristic frequency by controlling the overlap of the effective plasma frequency and I-SPP frequency. Region II in Fig. 6 is a forbidden band because of the single negative permeability of the (1,1) I-SPP, while region III is a double positive pass-band (see ESI for details). In addition, when the dielectric layer permittivity is just above 3.3, the maximum frequency for the (1,1) I-SPP is slightly lower than the effective plasma frequency, and both a high left-handed transmission and a high FOM are obtained [32].

Conclusions

In this work, the stacked fishnet structure was studied at optical wavelengths, and an analogous relationship between meta-atoms and real atoms was established on the basis of classic energy band theory in solid-state physics. The characteristic frequency of meta-atoms is equivalent to the energy level of real atoms. In an N-meta-atom

system, the characteristic frequency splits N times, similar to the energy level splitting for real atoms with a degeneracy of 1. The split characteristic frequency gradually forms a quasi-continuous band if the meta-atom number is large enough and the quasi-continuous band converges with increasing metal layer thickness i.e. equivalent atom spacing. The dielectric layer serves as the nucleus and its features also affect the equivalent energy bands. This work completes the physical picture for metamaterials and provides an understanding of the deeper physics of metamaterials from an equivalent atomic viewpoint. However, we should realize that there are still some differences between meta-atom and real atom, such as their electrical length/volume compared to the operating wavelength. The similarities and differences all enrich the understanding of metamaterial physics.

Acknowledgements

This work was supported by the National Youth Top-Notch Talent Support Program, the Program for New Century Excellent Talents in University (NCET-12-0780), the Fundamental Research Funds for the Central Universities, the Beijing Higher Education Young Elite Teacher Project (YETP0414).

Notes and References

1. G. Dolling, C. Enkrich, M. Wegener, C. M. Soukoulis and S. Linden, *Science*, 2006, 312, 892-894.
2. R. A. Shelby, D. R. Smith and S. Schultz, *Science*, 2001, 292, 77-79.
3. J. Valentine, S. Zhang, T. Zentgraf, E. Ulin-Avila, D. A. Genov, G. Bartal and X. Zhang, *Nature*, 2008, 455, 376-379.
4. C. M. Soukoulis and M. Wegener, *Nat. Photonics*, 2011, 5, 523-530.
5. J. Hao, Y. Yuan, L. Ran, T. Jiang, J. A. Kong, C. T. Chan and L. Zhou, *Phys. Rev. Lett.*, 2007, 99, 063908.
6. N. K. Grady, J. E. Heyes, D. R. Chowdhury, Y. Zeng, M. T. Reiten, A. K. Azad, A. J. Taylor, D. A. R. Dalvit and H. T. Chen, 2013, *Science*, 2013 340, 1304-1307.
7. N. Yu, P. Genevet, M. A. Kats, F. Aieta and J. P. Tetienne, *Science*, 2011, 334, 333-337.
8. C. Pfeiffer and A. Grbic, *Phys. Rev. Lett.*, 2013, 110, 197401.
9. S. Sun, Q. He, S. Xiao, Q. Xu, X. Li and L. Zhou, *Nat. Mater.*, 2012, 11, 426-431.
10. J. B. Pendry, *Phy. Rev. Lett.*, 2000, 85, 3966-3969.
11. N. Fang, H. Lee, C. Sun and X. Zhang, *Science*, 2005, 308, 534-537.
12. J. B. Pendry, D. Schurig and D. R. Smith, *Science*, 2006, 312, 1780-1782.
13. D. Schurig, J. J. Mock, B. J. Justice, S. A. Cummer, J. B. Pendry, A. F. Starr and D. R. Smith, *Science*, 2006, 314, 977-980.
14. L. H. Gabrielli, J. Cardenas, C. B. Poitras and M. Lipson, *Nat. Photonics*, 2009, 3, 461-463.

15. C. Hu, Z. Zhao, X. Chen and X. Luo, *Opt. Express*, 2009, 17, 11039-11044.

16. H. T. Chen, *Opt. Express*, 2012, 20, 7165-7172.

17. J. B. Pendry, *Contemp. Phys.*, 2004, 45, 191-202.

18. C. Rockstuhl, C. Menzel, S. Mühlig, J. Petschulat, C. Helgert, C. Etrich, A. Chipouline, T. Pertsch and F. Lederer, *Phys. Rev. B*, 2011, 83, 245119.

19. N. Liu, S. Kaiser and H. Giessen, *Adv. Mater.*, 2008, 20, 4521-4525.

20. N. Liu, H. Guo, L. Fu, S. Kaiser, H. Schweizer and H. Giessen, *Adv. Mater.*, 2007, 19, 3628-3632.

21. C. García-Meca, R. Ortuño, F. J. Rodríguez-Fortuño, J. Martí and A. Martínez, *Opt. Lett.*, 2009, 34, 1603-1605.

22. A. Mary, S. G. Rodrigo, F. J. Garcia-Vidal and L. Martin-Moreno, *Phys. Rev. Lett.*, 2008, 10, 103902.

23. C. García-Meca, R. Ortuño, F. J. Rodríguez-Fortuño, J. Martí and A. Martínez, *Opt. Express*, 2009, 17, 6026-6031.

24. E. N. Economou, *Phys. Rev.*, 1969, 182, 539-554.

25. R. Ortuño, C. García-Meca, F. J. Rodríguez-Fortuño, J. Martí and A. Martínez, *Phys. Rev. B*, 2009, 79, 075425.

26. T. W. Ebbesen, H. J. Lezec, H. F. Ghaemi, T. Thio and P. A. Wolff, *Nature*, 1998, 391, 667-669.

27. R. G. Heideman, P. V. Lambeck and J. G. E. Gardeniers, *Opt. Mater.*, 1995, 4, 741-755.

28. X. Chen, T. M. Grzegorczyk, B.-I. Wu, J. Pacheco and J. A. Kong, *Phys. Rev. E*, 2004, 70, 016608.

29. D. R. Smith, S. Schultz, P. Markoš and C. M. Soukoulis, *Phys. Rev. B*, 2002, 65, 195104.

30. T. Li, J.Q. Li, F.M. Wang, Q.J. Wang, H. Liu, S. N. Zhu and Y. Y. Zhu, *Appl. Phys. Lett.*, 2007, 90, 251112.

31. T. Li, H. Liu, F. M. Wang, J. Q. Li, Y. Y. Zhu and S. N. Zhu, *Phys. Rev. E*, 2007, 76, 016606.

32. S. Zhang, W. Fan, N. C. Panoiu, K. J. Malloy, R. M. Osgood and S. R. Brueck, *Opt. Express*, 2006, 14, 6778-6787.

Figure Captions.

Fig. 1. Schematics for a one-dimensional fishnet structure and a single unit cell.

Fig. 2. Electromagnetic characteristics of one meta-atom. (a) Transmission (red), reflection (black) and absorption (green) amplitudes. (b)-(e) Real (black) and imagery (red) parts of the extracted n_{eff}, Z_{eff}, μ_{eff}, and ε_{eff}. The blue and red regions indicate double-negative and single-negative regions, respectively. The purple and black dashed lines indicate ω_{ep} and localized resonance, respectively. (f) H_y distribution maps for frequencies of 401 THz, 507 THz and 650 THz for the middle plane of the dielectric layer. SPP dispersion relation of a single-layer fishnet structure (g) and two-layer fishnet structure (h).

Fig. 3. Electromagnetic characteristics of multiple meta-atoms. The transmission (red), reflection (black) and absorption (green) amplitudes for (a) two, (b) three, (c) four, and (d) five meta-atoms. (e) Characteristic frequency as a function of meta-atomic number.

Fig. 4. Effect of meta-atomic number. (a) Contour plot of the reflection amplitude vs. meta-atomic number and frequency. The dashed line represents ω_{ep}. (b) Schematic of the effective energy level splitting with increasing meta-atomic number. (c) H_y distribution maps for $\left|\boldsymbol{f}_{5M}\right\rangle$ of (1,0) I-SPP (upper) and (1,1) I-SPP (lower) in the yz-plane for five meta-atoms.

Fig. 5. Effect of meta-atomic spacing. (a) Characteristic frequency as a function of meta-atomic spacing D for five meta-atoms. The intersecting part of two characteristic bands is represented by the hollow shapes and the H_y distribution maps are shown on the left (D=62 nm and *f*=458 THz). (b) Contour plot of the reflection amplitude vs. meta-atomic spacing and frequency. The submode discontinuity was caused by simulation meshing. The insert displays the energy band structure of a silicon crystal vs. the atomic spacing.

Fig. 6. Effect of dielectric layer permittivity. Contour plot of the transmission amplitude vs. dielectric layer permittivity and frequency for 27 meta-atoms (D=82 nm).

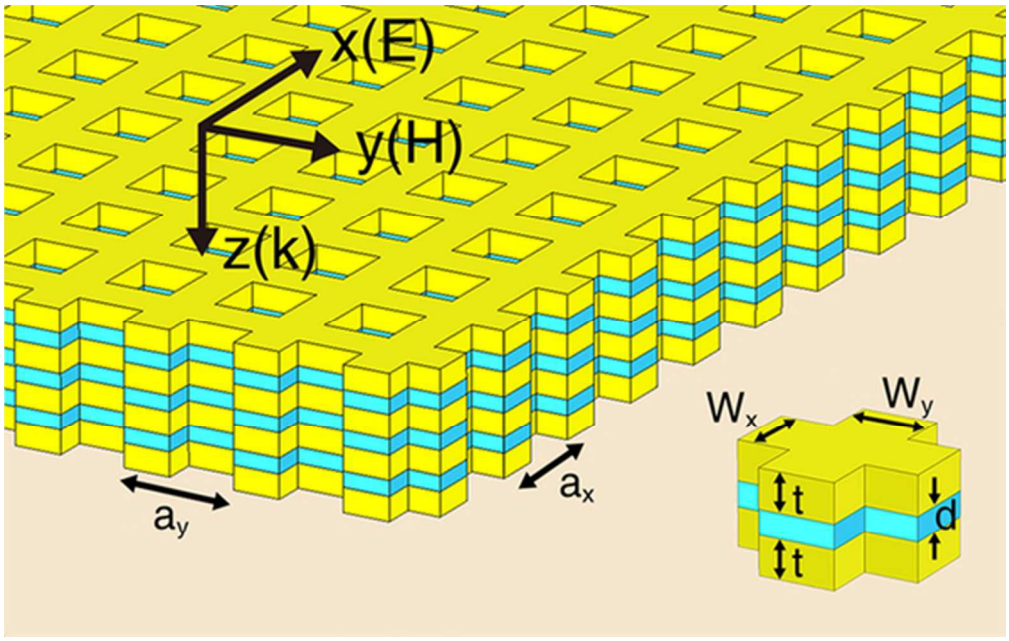

50x31mm (300 x 300 DPI)

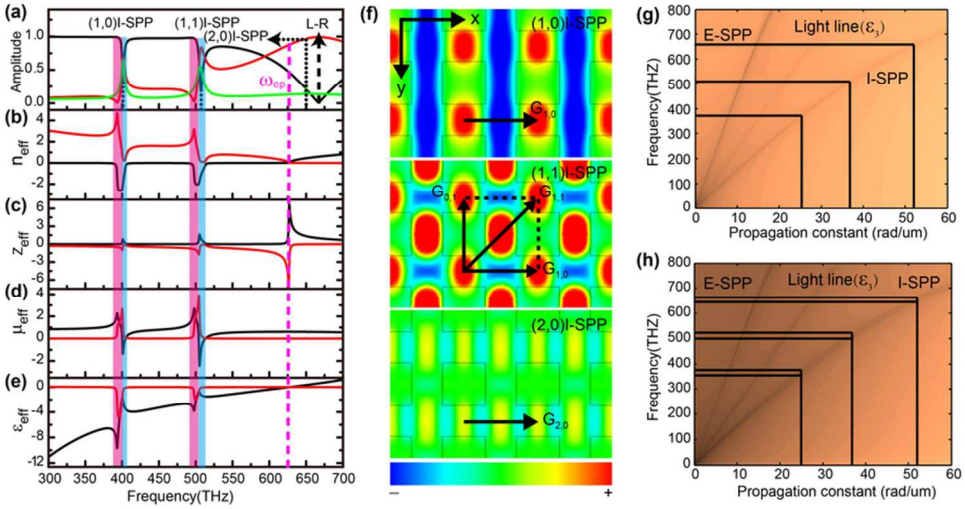

80x42mm (300 x 300 DPI)

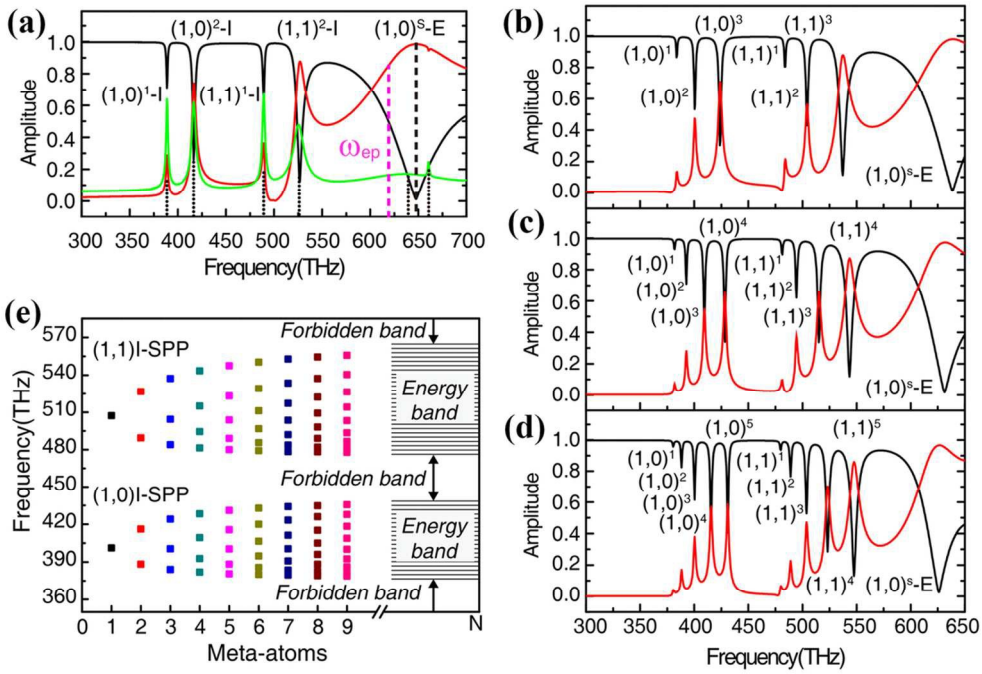

106x74mm (300 x 300 DPI)

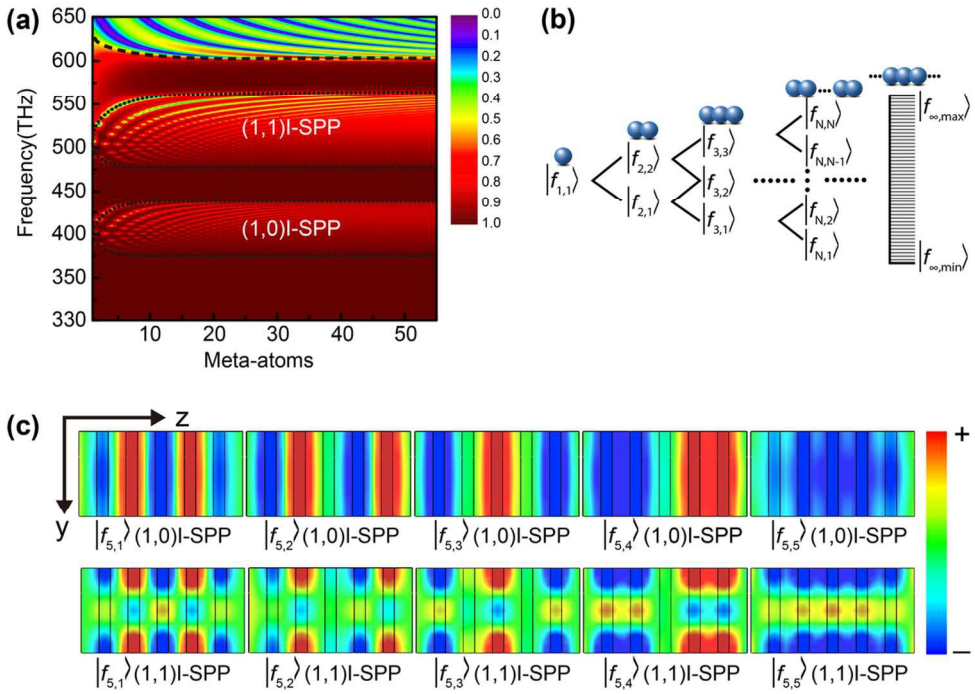

109x79mm (300 x 300 DPI)

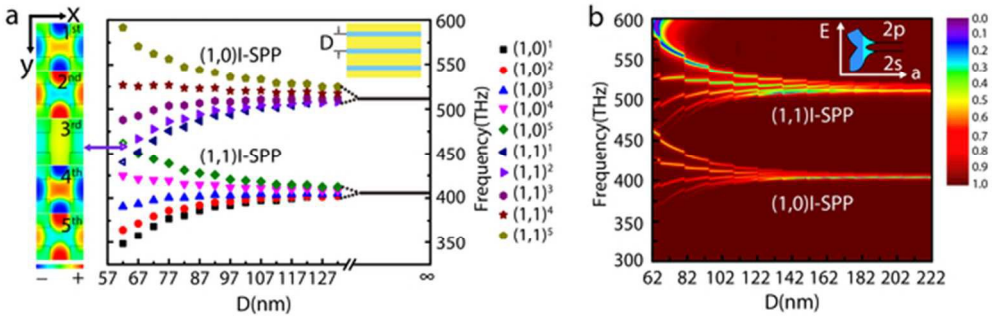

55x18mm (300 x 300 DPI)

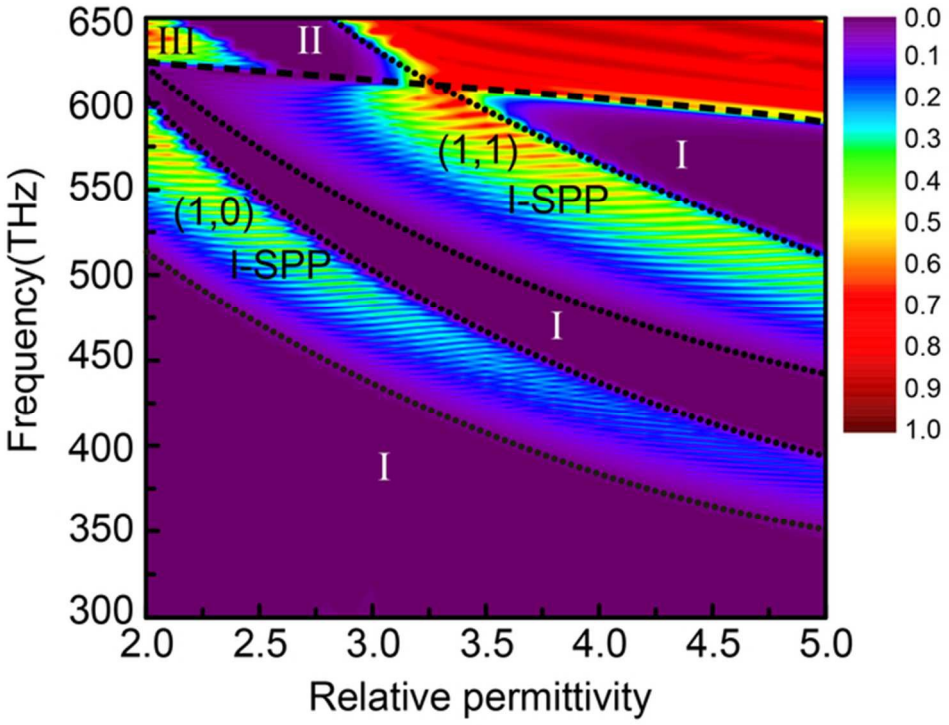

59x44mm (300 x 300 DPI)

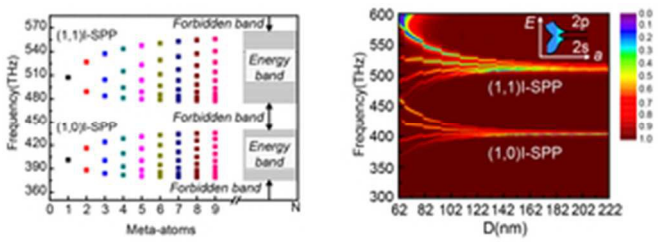

27x10mm (300 x 300 DPI)